Spatio-Temporal Analysis of Induced	Seismicity and Infrastructure Risk in Oklahoma
	Chenyi Weng
SSCI575	- Spatial Data Science
Pı	rofessor Yi Qi
Oct	tober 7th, 2025

### 1. Spatial Data Representation and Wrangling

### 1 (a) Enabling and Displaying the Spatio-Temporal Pattern

To visualize the spatio-temporal pattern of earthquake and water-injection activity in Oklahoma, both datasets were first projected into the same coordinate system to ensure spatial consistency. The Project tool in ArcGIS Pro was used to convert *OK\_earthquakes\_Project* and *OK\_well\_injection\_Project* to *NAD 1983 UTM Zone 14N*, as shown in *Figure 1* and *Figure 2*. This projection ensures accurate measurement of distances and alignment between the two layers, which is essential for later spatial comparison and cube generation.

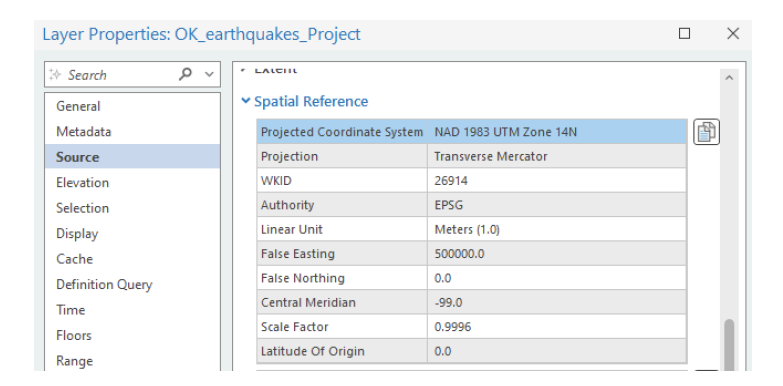


Figure 1. Project tool settings for OK earthquakes Project to NAD 1983 UTM Zone 14N.

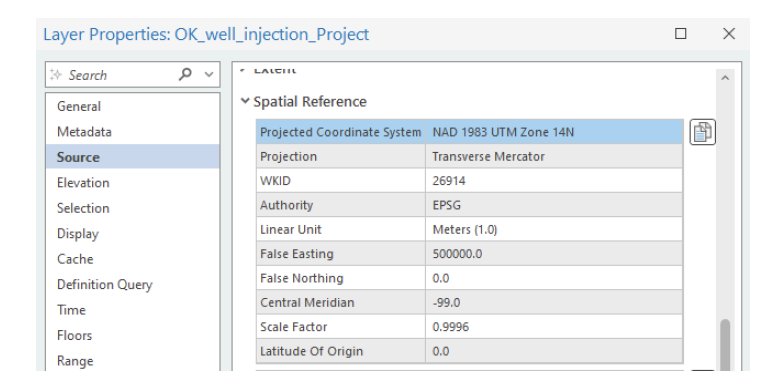


Figure 2. Project tool settings for OK\_well\_injection\_Project to NAD 1983 UTM Zone

After projection, the attribute table of *OK\_earthquakes\_Project* was examined, and the *updated\_Converted* field was confirmed as the temporal variable. Two one-year intervals, 2013 and 2017, were chosen to illustrate changes in earthquake locations over time. The one-year interval was selected because it provides a clear comparison of spatial distributions across different periods while maintaining adequate temporal detail. Using Select By Attributes, records were filtered with SQL expressions such as "*updated\_Converted*" >= DATE '2013-01-01' AND "*updated\_Converted*" > DATE '2014-01-01' and "*updated\_Converted*" >= DATE '2017-01-01' AND "*updated\_Converted*" > DATE '2018-01-01'.

The results are displayed in *Figure 3* and *Figure 4*. In 2013, earthquake events were mostly concentrated in the northern and eastern regions of Oklahoma, whereas by 2017 the activity had expanded toward the central part of the state. These changes reveal a clear spatial expansion of seismic activity that may correspond to increased subsurface fluid-injection operations during that period.

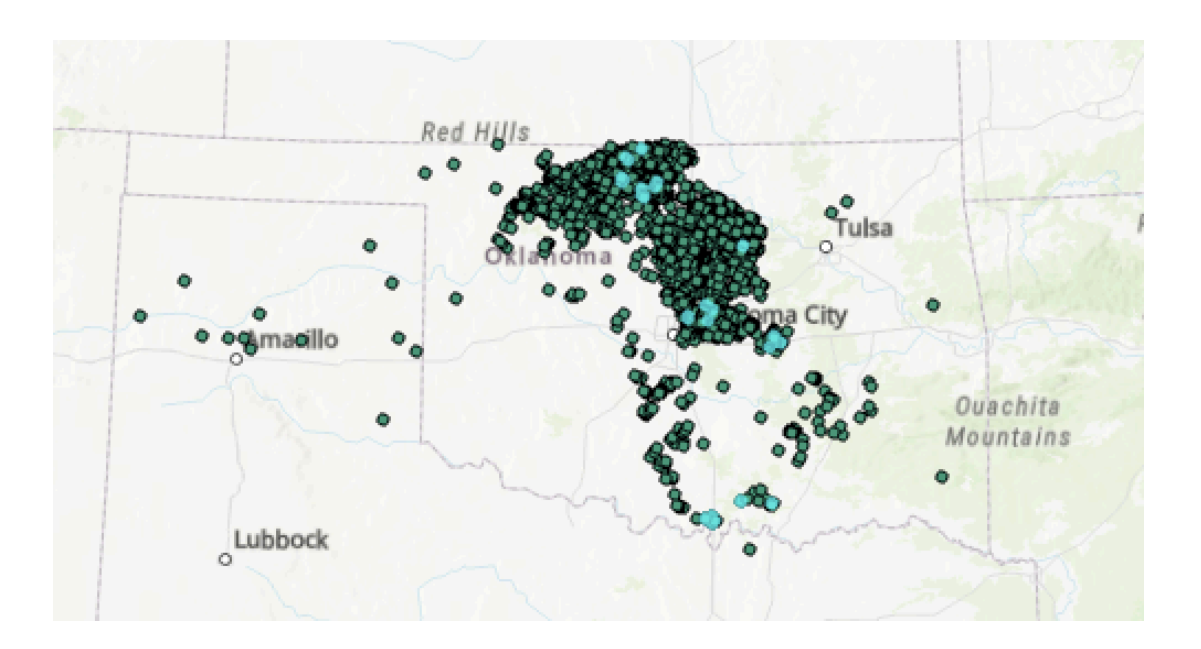


Figure 3. Earthquakes in 2013

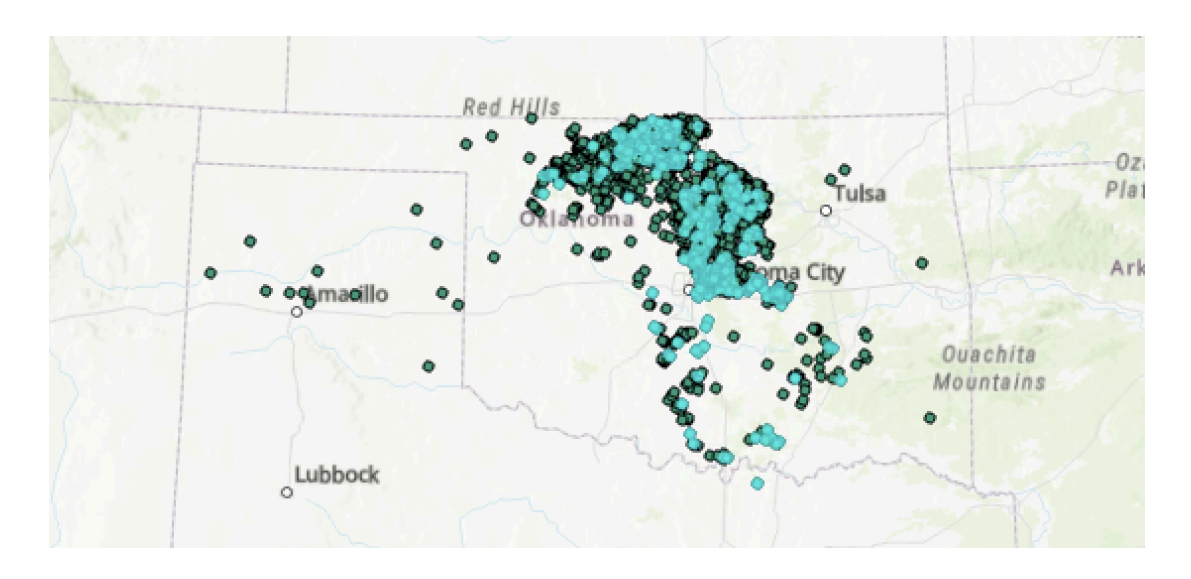


Figure 4. Earthquakes in 2017

# 1 (b) Identifying Fields with Missing Data

A detailed review of both datasets was conducted to identify fields containing missing or incomplete data. In the earthquake dataset, the field nst, which represents the number of seismic stations used to determine each event, contained several NULL values. These missing records are visible in *Figure 5*. Missing nst values typically occur when small-magnitude earthquakes are recorded by too few sensors or when station data are incomplete.

	OK_earthquakes_Project × OK_well_injection_Project										
Field	Field: 🚃 👨 Selection: 🖺 🦪 🖺 🗐										
e *	e * time   latitude   longitude   depth   mag   magType   nst   gap   dmin   rms   net									net	
1	2016-07-24T23:36:06.9	36.4513	-98.7711	7.745	3.1	ml	<null></null>	59	<null></null>	0.59	us
2	2016-07-24T23:10:24.7	36.5866	-98.5436	7.22	2.5	ml	<null></null>	44	<null></null>	0.48	us
3	2016-07-24T09:03:15.9	36.1281	-97.1018	3.499	2.5	ml	<null></null>	51	<null></null>	0.63	us
4	2016-07-24T08:59:00.4	36.1303	-97.0973	6.131	2.6	ml	<null></null>	52	<null></null>	0.6	us
5	2016-07-24T08:09:07.0	36.1281	-97.0977	5.922	3	ml	<null></null>	51	<null></null>	0.22	us
6	2016-07-24T04:45:17.2	36.8449	-98.8036	5.699	2.5	ml	<null></null>	116	<null></null>	0.48	us
7	2016-07-24T03:08:41.0	36.5874	-98.5408	7.015	2.9	ml	<null></null>	44	<null></null>	0.43	us

Figure 5. Missing values (NULL) in the nst field of OK earthquakes Project

In the water injection dataset, the field *Volume\_BPD* contained a large number of zero values that do not represent true measurements but rather missing or unreported injection volumes. These pseudo-missing values are shown in *Figure 6*. Although technically valid numeric entries, the zeros could bias later analyses by under-representing injection intensity. Identifying these two problematic fields was an important step to ensure data quality before temporal aggregation and cube construction.

⊞ ок_	■ OK_earthquakes_Project    ■ OK_well_injection_Project ×								
Field:	Field: 🕎 🗒 Selection: 🖺 🍕 📳 🗒 🚭								
4	Name Well_Number Operator_Number Report_Date Volume_BPD Pressure API_NUM								
466771	SON 22-18N-2E	'1SWD	20751	2015-07-29 00:00:00.000	0	1	4158		
466772	SON 22-18N-2E	'1SWD	20751	2015-07-28 00:00:00.000	0	1	4158		
466773	SON 22-18N-2E	'1SWD	20751	2015-07-27 00:00:00.000	0	1	4158		
466774	SON 22-18N-2E	'1SWD	20751	2015-07-26 00:00:00.000	0	1	4158		
466775	SON 22-18N-2E	'1SWD	20751	2015-07-25 00:00:00.000	0	1	4158		
466776	SON 22-18N-2E	'1SWD	20751	2015-07-24 00:00:00.000	0	1	4158		
466777	SON 22-18N-2E	'1SWD	20751	2015-07-23 00:00:00.000	0	1	4158		

Figure 6. Zero (pseudo-missing) values in the Volume\_BPD field of OK\_well\_injection\_Project

# 1 (c) Fixing the Missing Data and Justifying the Approach

To address the missing and pseudo-missing values, the Field Calculator was used to create corrected fields. For the earthquake dataset, a new field named *nst\_fixed* was added. The Python expression "*I if !nst! is None else !nst!*" was applied to replace NULL values with 1, since every earthquake event should be recorded by at least one seismic station. The Field Calculator setup is illustrated in *Figure 7*. This correction guarantees that all events maintain valid station counts, avoiding data gaps that might affect magnitude statistics or clustering analyses.

III OK_earthquakes_Project × III OK_well_injection_Project III Fields: OK_earthquakes_Project ∨									
Field: □ Selection: □ □ □ □ □ □ □ □ □									
- 4	Nst	status	locationSource	magSource	updated_Converted	nst_fixed	^		
4487	ıll>	reviewed	tul	tul	1/31/2015 2:50:16 AM	<null></null>			
4488	ıll>	reviewed	tul	tul	1/31/2015 2:50:16 AM	<null></null>			
4489	ıll>	reviewed	tul	tul	7/14/2017 8:51:00 PM	1			
4490	ıll>	reviewed	tul	tul	1/31/2015 2:50:15 AM	<null></null>			
4491	ıll>	reviewed	tul	tul	1/31/2015 2:50:15 AM	<null></null>			
4492	ıll>	reviewed	tul	tul	7/14/2017 8:51:19 PM	1	•		
4493	ıll>	reviewed	tul	tul	1/31/2015 2:50:14 AM	<null></null>			
4494	ıll>	reviewed	tul	tul	7/14/2017 8:51:36 PM	1	V		
<	<								

Figure 7. Field calculation setup for nst\_fixed showing Python expression replacing NULL values

For the water-injection dataset, a new field named *Volume\_fixed* was created to replace unrealistic zeros in the *Volume\_BPD* field. The average injection volume, 2886.476683 barrels per day, was calculated and substituted for zero values using the Python expression "2886.476683 if!Volume\_BPD! == 0 else!Volume\_BPD!", as displayed in *Figure 8*. Using the mean value as a replacement preserves the dataset's central tendency and prevents underestimation of injection intensity caused by missing reports. Because the missing entries were scattered randomly across both time and space, interpolation or regression would not have produced more reliable results. This simple but robust imputation method maintains the overall data distribution and supports consistent statistical analysis.

■ OK_earthquakes_Project    ■ OK_well_injection_Project ×      ■ OK_well_injection_Project ×									
Field:	Field: 🖽 🖽   Selection: 🖫 📲 🗒 🗒								
	Well_Number	Operator_Number	Report_Date	Volume_BPD	Pressure	API_NUM	Volume_fixed	^	
113611	'1 SWD	20585	2017-07-03 00:00:00.000	3043	300	3499	3043		
113612	'1 SWD	20585	2017-07-02 00:00:00.000	9918	300	3499	9918	U	
113613	'1 SWD	20585	2017-07-01 00:00:00.000	7322	0	3499	7322		
113614	'1 SWD	20585	2017-06-30 00:00:00.000	0	0	3499	2886.476683		
113615	'1 SWD	20585	2017-06-29 00:00:00.000	10450	180	3499	10450		
113616	'1 SWD	20585	2017-06-28 00:00:00.000	9201	310	3499	9201		
113617	'1 SWD	20585	2017-06-27 00:00:00.000	9812	390	3499	9812		
113618	'1 SWD	20585	2017-06-26 00:00:00.000	8540	220	3499	8540		
<	<								

Figure 8. Field calculation for Volume fixed showing replacement of 0 with mean value

After these modifications, both datasets contained continuous numeric values suitable for temporal aggregation. The cleaned datasets are now ready for the creation of space time cubes and subsequent spatial-temporal analyses. These preprocessing steps improve data integrity, minimize bias, and ensure compatibility between the earthquake and injection datasets for further correlation studies.

### 2. Representing Spatio-Temporal Data

### 2 (a) Oklahoma Earthquake Space Time Data Structure

To represent the spatio-temporal distribution of earthquake events in Oklahoma, the Create Space Time Cube by Aggregating Points tool in ArcGIS Pro was employed. The input dataset, *OK\_earthquakes\_Project*, contained temporal information stored in the *updated\_Converted* field. A space-time cube was generated as a NetCDF file (*OK\_earthquakes\_cube.nc*) with a temporal resolution of three months and a spatial grid size of  $10 \times 10$  kilometers using the fishnet shape type. Each grid cell aggregates the mean earthquake

magnitude values occurring within its spatial boundary during each three-month period. This configuration ensures that the dataset includes at least ten temporal slices, providing sufficient temporal depth to capture both short-term fluctuations and long-term trends in seismic activity.

The chosen three-month interval helps smooth irregular earthquake occurrences while maintaining enough temporal detail to detect seasonal variations. Likewise, the 10 km fishnet grid provides an appropriate balance between spatial precision and computational efficiency. It is fine enough to distinguish localized clusters while broad enough to avoid fragmentation of sparse events. The resulting cube establishes a consistent framework for spatio-temporal analysis, allowing for systematic examination of how earthquake activity has evolved across the state over time. This structure will later support analyses such as trend detection and hot spot mapping.

As illustrated in *Figure 9*, the ArcGIS tool interface displays the parameter configuration used to build the space-time cube, including the three-month interval and 10 km fishnet aggregation. *Figure 10* presents a 2D visualization of the earthquake cube. Each gray cell represents a  $10 \times 10$  km grid aggregated over three months, summarizing average earthquake magnitudes throughout Oklahoma. The visualization reveals spatial clusters of higher activity in north-central and southern regions of the state, indicating potential fault zones where earthquakes occur more frequently.

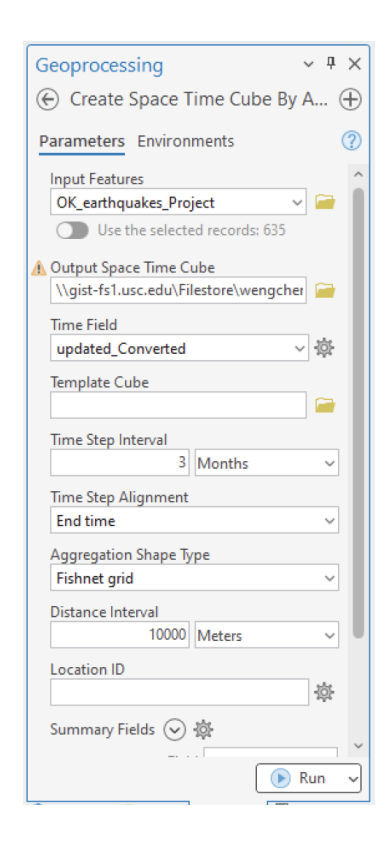


Figure 7. Tool setup for creating the Oklahoma earthquake space time cube

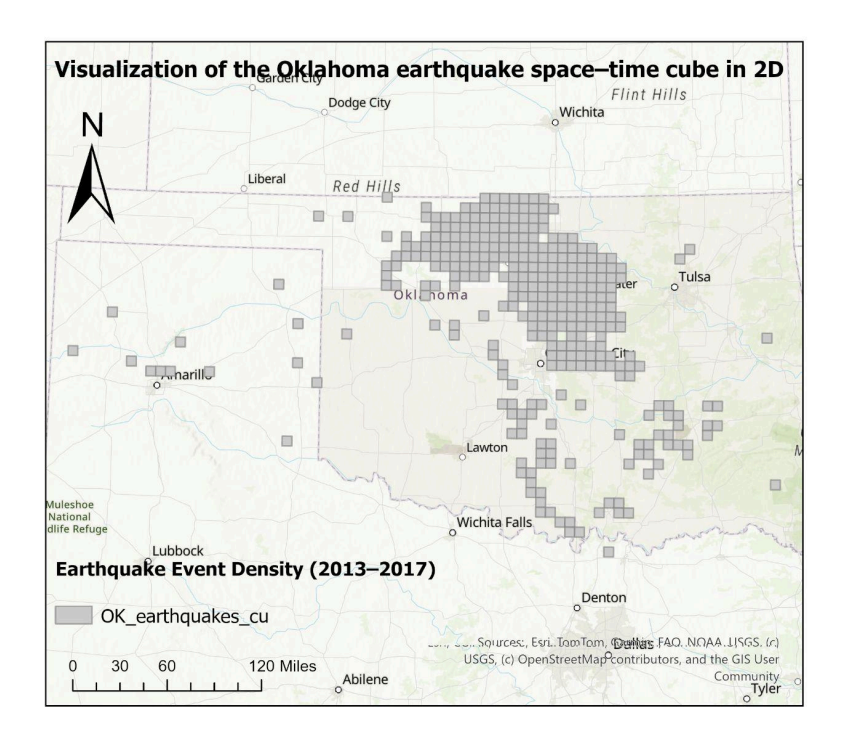


Figure 8. Visualization of the Oklahoma earthquake space time cube in 2D

### 2 (b) Oklahoma Water Injection Space—Time Data Structure

A parallel space-time representation was constructed for the water injection dataset  $OK\_well\_injection\_Project$  to enable direct comparison with the earthquake data. Before generating the cube, two key attribute fields were created to ensure correct temporal and numerical formatting. First, a new date field named  $Report\_Date\_Converted$  was derived from the original  $Report\_Date$  field to store proper date values. Second, a numeric (double) field named  $Volume\_BPD\_Fixed$  was calculated to represent daily injection volumes as floating-point numbers. These pre-processing steps ensured that the cube tool could interpret both temporal and quantitative attributes accurately.

The Create Space Time Cube by Aggregating Points tool was then applied using Report\_Date\_Converted as the time field and Volume\_BPD\_Fixed as the summary field. Each cube bin covered a 10 × 10 km grid cell and aggregated data at a three-month interval, consistent with the earthquake cube. The summary statistic was set to Mean, and empty bins were filled with zeros to preserve temporal continuity. This configuration captures both spatial distribution and seasonal variation in injection activity while minimizing bias from missing records. The three-month interval also corresponds to typical industry reporting cycles for injection operations, ensuring that temporal aggregation aligns with operational patterns.

As shown in *Figure 11*, the parameter settings for the water injection cube mirror those of the earthquake cube to maintain analytical consistency. *Figure 12* illustrates the 2D visualization of the water injection space-time cube. Each gray grid cell indicates the average injection volume aggregated over three-month periods. The spatial pattern highlights major injection regions

across northern and central Oklahoma, revealing the geographical concentration of high-volume injection wells.

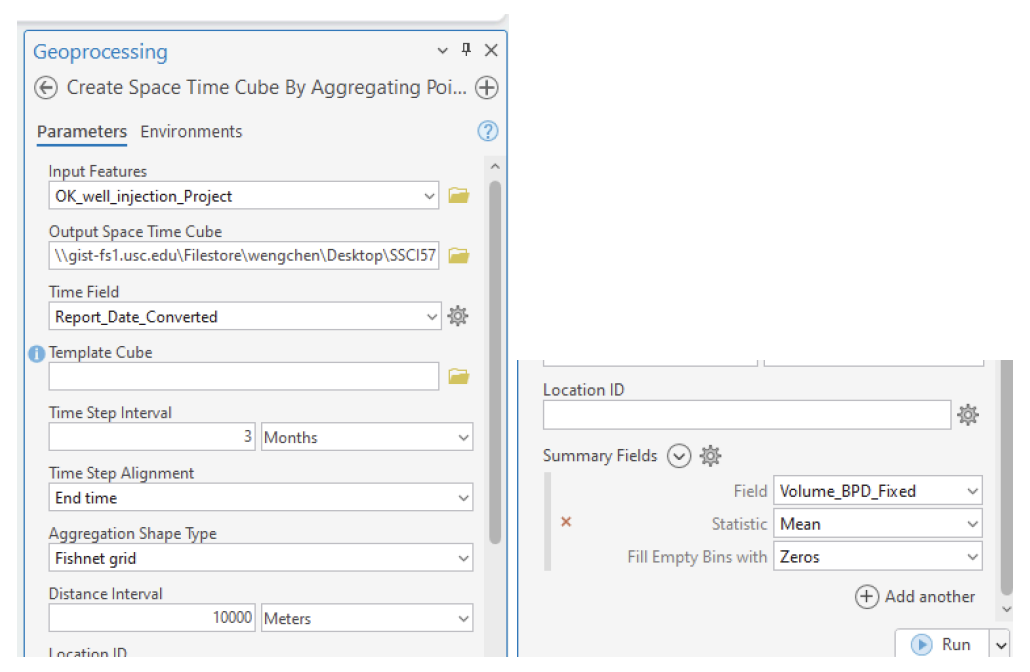


Figure 11. Tool setup for creating the Oklahoma well injection space time cube

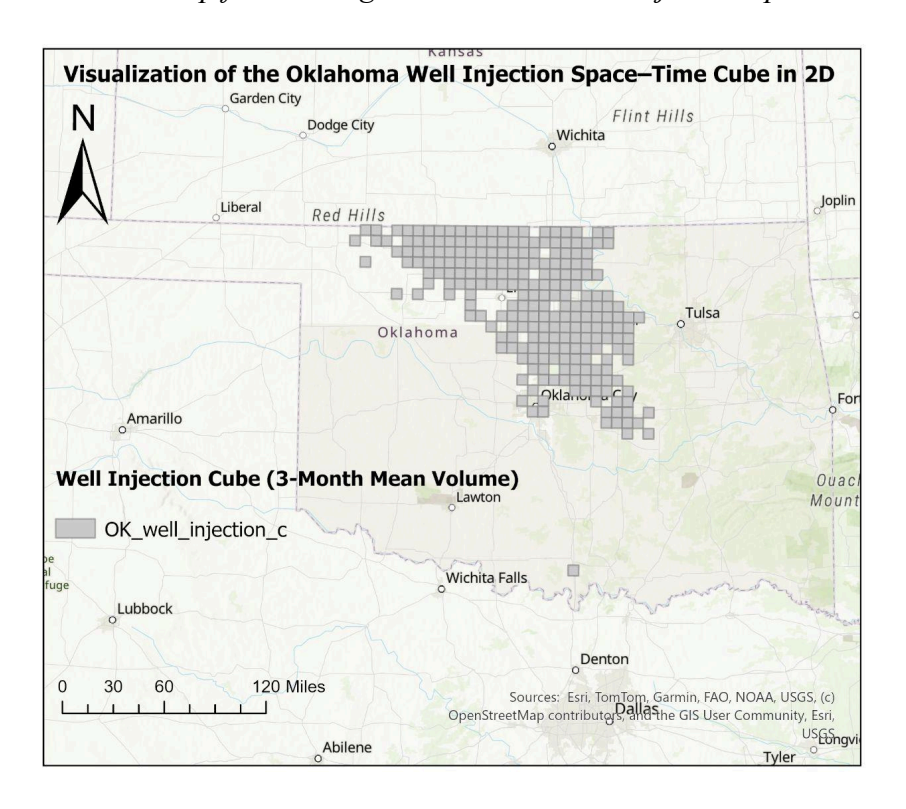


Figure 12. Visualization of the Oklahoma well injection space time cube in 2D

The consistent design of the two space-time cubes, both with 10 km spatial resolution and three-month temporal intervals, enables direct spatial and temporal correlation between seismic activity and injection intensity. This balanced structure offers adequate detail for trend identification while maintaining computational efficiency for subsequent analyses such as emerging hot spot detection and cross-cube comparison. The uniform cube configuration ensures that the patterns derived from both datasets can be compared meaningfully within the same spatial and temporal framework.

#### 3. Data Visualization

## 3 (a) Temporal Distribution of Earthquakes and Water Injection Records (2013–2017)

The temporal distribution of earthquake occurrences and water injection activities in Oklahoma between 2013 and 2017 was examined to understand how both phenomena changed over time. *Figure 13* presents a histogram of earthquake occurrences by year. The figure shows that seismic activity was relatively low in 2013 and 2014, followed by a sharp increase that peaked in 2015 and 2016, before declining again in 2017. The overall distribution forms a unimodal pattern centered around 2015, indicating that the middle years of the study period experienced the highest frequency of earthquakes.

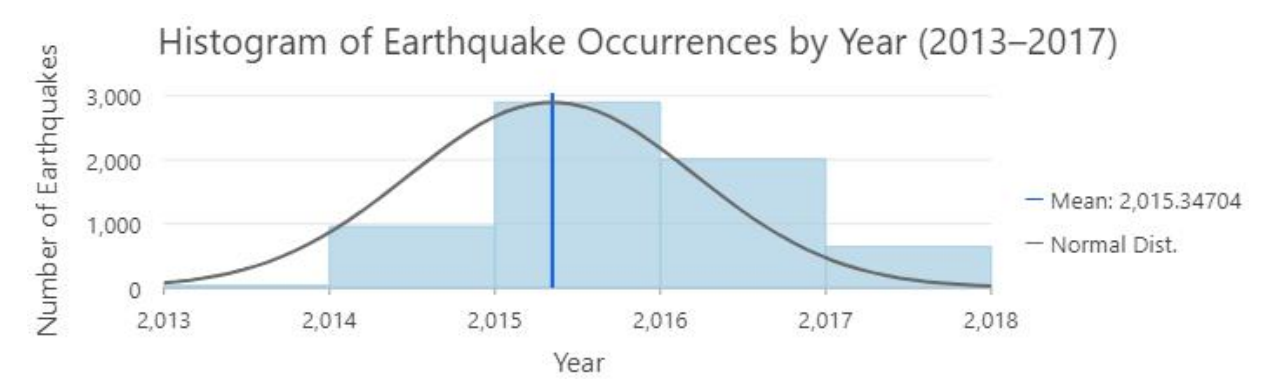


Figure 13. Histogram of Earthquake Occurrences by Year (2013–2017)

Figure 14 displays the annual frequency of water injection records over the same period. The number of injection operations rose steadily after 2014, reaching its maximum in 2016 and 2017, and then decreased noticeably in 2018. This pattern demonstrates a period of intensified water injection activities in the mid 2010s, consistent with an overall expansion of oil and gas operations that relied on underground fluid disposal.

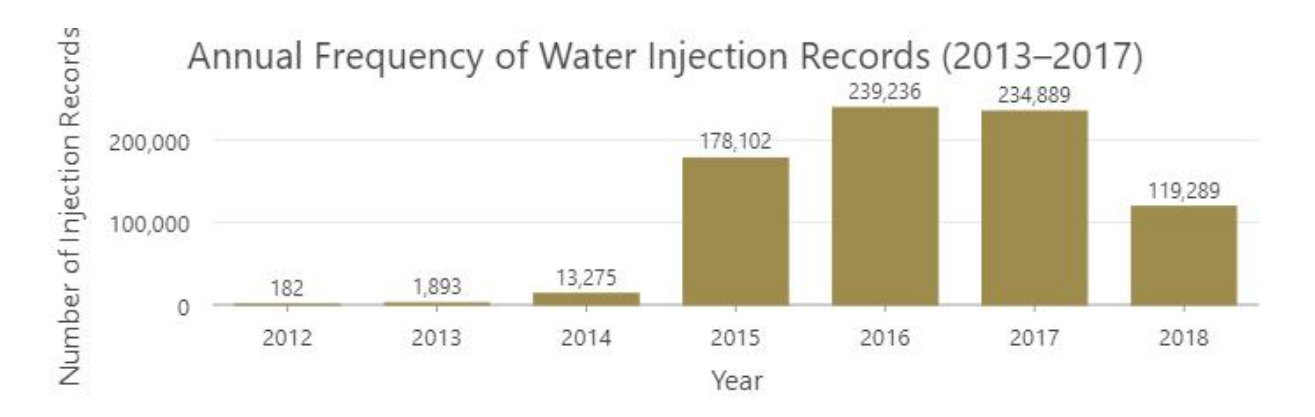


Figure 14. Annual Frequency of Water Injection Records (2013–2017)

When comparing *Figure 13* and *Figure 14*, a similar temporal trend can be observed between the two datasets. Both the earthquake occurrences and water injection activities reached their respective peaks around 2015–2016 and declined afterward. This resemblance in timing suggests a potential temporal correlation between increased injection operations and higher seismic activity during the study period. While this analysis does not establish causation, it highlights a clear synchronization between the intensification of human-induced subsurface activities and the rise in earthquake frequency, providing a foundation for further spatial and statistical analyses in the subsequent sections.

### 3 (b) Data Clock Visualization for Earthquake Magnitude and Water Injection Rate

The data clock visualizations were produced to examine the temporal patterns of earthquake magnitude and water injection rate in Oklahoma from 2013 to 2017. The first data

clock, shown in *Figure 15*, illustrates the distribution of average earthquake magnitude over time. The rings represent years, while the wedges represent months. Darker blue shades indicate periods with higher mean earthquake magnitudes. The figure shows that seismic activity increased notably in 2015 and 2016, with slightly stronger magnitudes concentrated in the summer and early autumn months, suggesting seasonal variations in seismic behavior during the mid-study period.

# Data Clock of Earthquake Magnitude (2013–2017)



Figure 15. Data Clock of Earthquake Magnitude (2013-2017)

The second data clock, presented in *Figure 16*, depicts the mean water injection rate for the same period. Similar to the earthquake data, the rings denote years and the wedges denote months, with darker blue tones indicating higher injection volumes. The data clock reveals that water injection rates peaked between 2015 and 2016 and remained relatively high through 2017. The gradual color intensification from 2014 to 2016 reflects an increasing injection activity pattern across both time and season.

# Data Clock of Water Injection Rate (2013–2017)

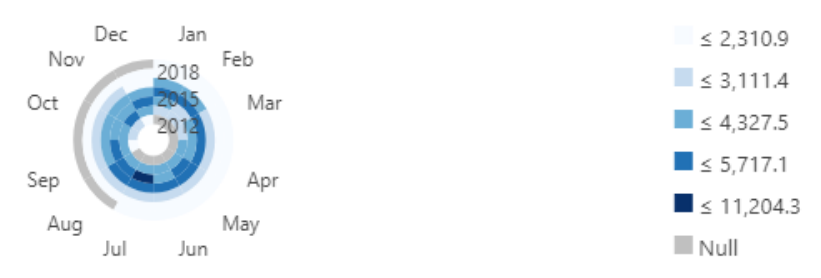


Figure 16. Data Clock of Water injection Rate (2013-2017)

When comparing the two visualizations, both exhibit elevated activity in 2015 and 2016, suggesting a temporal overlap between higher injection rates and increased seismic magnitudes. This synchronicity provides preliminary evidence of a potential relationship between fluid injection intensity and regional seismic responses over time.

# 3 (c) Space-Time Trend Visualization for Water Injection Data

To analyze long-term spatial and temporal patterns in both earthquake activity and water injection operations across Oklahoma from 2013 to 2017, the *Visualize Space Time Cube in 2D* tool was applied to the two datasets. The input files included the earthquake space-time cube (*OK\_earthquakes\_cube.nc*) and the water injection cube (*OK\_well\_injection\_cube.nc*). For the earthquake cube, the variable *COUNT* was used to represent the frequency of events within each 10-kilometer grid cell. For the water injection cube, the variable *VOLUME\_BPD\_FIXED\_MEAN\_ZEROS* was selected to represent the average daily injected volume of fluid. The *Trends* display theme was chosen in both cases to detect the overall temporal changes in each location.

Each output layer was visualized using graduated color symbology based on the *Trend z-score* field. The *Natural Breaks (Jenks)* classification method with five color classes was applied, ranging from yellow (representing decreasing or stable trends) to red (indicating increasing trends). The earthquake trend map (Figure 17) shows clusters of positive z-scores concentrated in central and northern Oklahoma, suggesting areas with a consistent increase in earthquake frequency over time. Similarly, the water injection trend map (Figure 18) reveals strong positive z-scores in the same regions, particularly around north-central Oklahoma, where injection volumes have significantly increased.

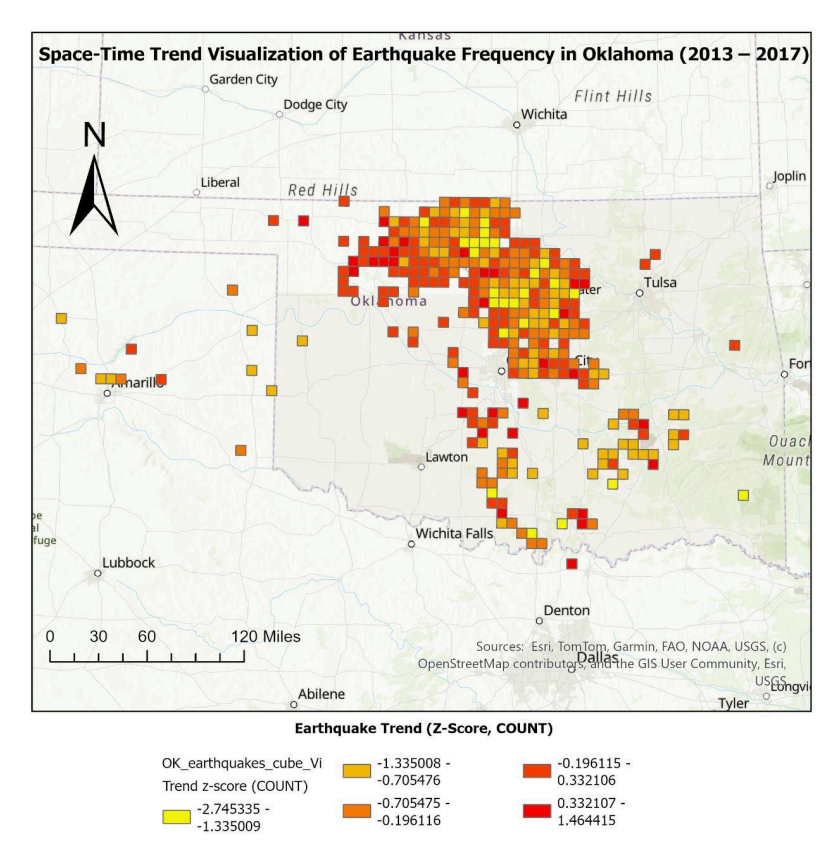


Figure 17. Space-Time Trend Visualization of Earthquake Frequency in Oklahoma (2013–2017)

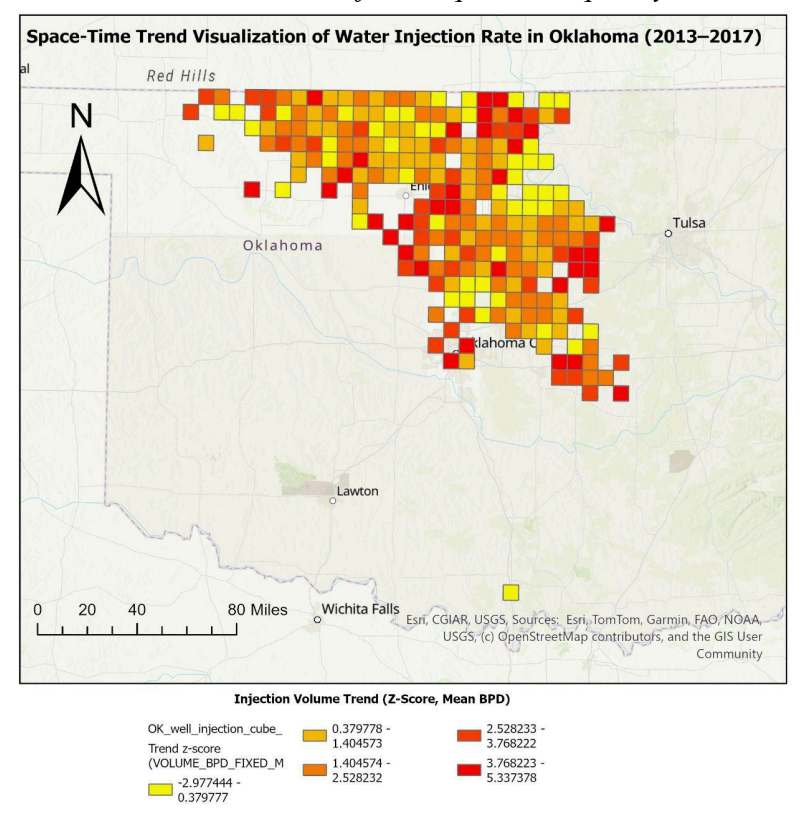


Figure 18. Space-Time Trend Visualization of Water Injection Rate in Oklahoma (2013–2017)

The spatial overlap of upward trends in both injection rate and earthquake frequency highlights a potential relationship between increased wastewater injection activity and elevated seismic occurrences. These findings visually reinforce the temporal correlation between human-induced subsurface fluid injection and the surge in earthquake events observed during the mid-2010s.

# 3 (d) Time Series Pattern Analysis

The selected study area focuses on Central Oklahoma, which includes Oklahoma City and surrounding counties, an area recognized for significant induced seismicity between 2013 and 2017. *Figure 19* shows the monthly variation of mean earthquake magnitude derived from the layer *EQ\_CentralOK\_Selected*. The time series reveals relatively stable and low magnitudes from 2013 to 2015 (around 2.8–3.0), followed by a sharp increase in 2016 and 2017, when several events exceeded magnitude 4. This pattern indicates a notable escalation of seismic activity in the later years.

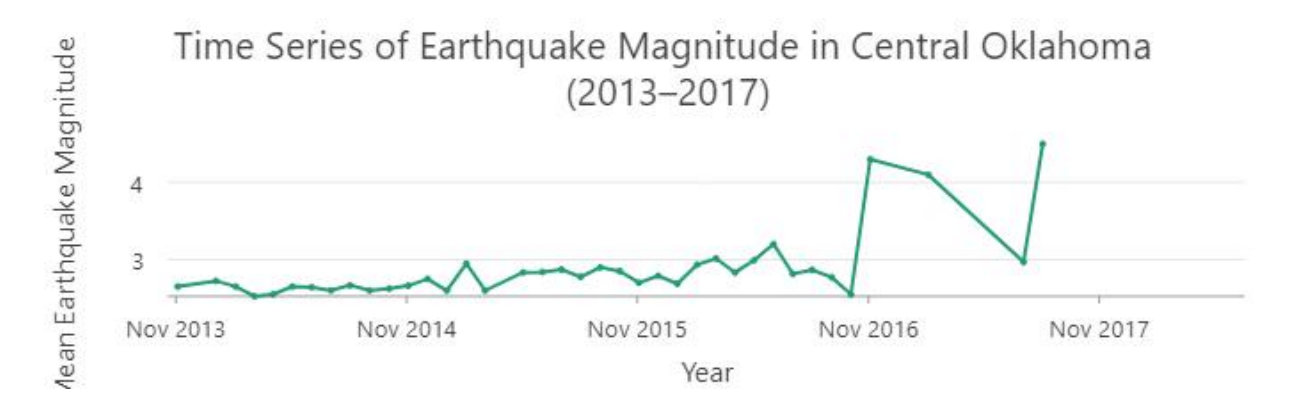


Figure 19. Time Series of Earthquake Magnitude in Central Oklahoma (2013–2017)

Figure 20 displays the average monthly water injection rate extracted from

Injection CentralOK Selected. From 2013 to 2014, the injection rate exceeded 20,000 barrels

per day but decreased steadily through 2015 and dropped sharply around mid-2016, remaining at a low and stable level thereafter. Comparing the two charts, a negative temporal relationship can be observed: while the injection rate declined significantly after 2015, the earthquake magnitude increased during 2016 and 2017. This inverse trend suggests that changes in injection practices may have altered subsurface stress conditions, contributing to short-term fluctuations in seismic activity.



Figure 20. Time Series of Water Injection Rate in Central Oklahoma (2013–2017)

### 4. Calculating earthquake risk in 2010.

# 4 (a) Select and merge all data sources for 2010 at the census tract level

To prepare the data for the earthquake risk analysis in 2010, all datasets were first projected to a consistent coordinate system, NAD 1983 UTM Zone 14N, to ensure spatial alignment. The datasets included four major layers: earthquake occurrences, water injection wells, school locations, and traffic volume points. Each dataset was clipped to the boundary of the Oklahoma census tracts using the Clip tool, with the 2010 census tract layer (*census\_tracts10\_Project*) serving as the boundary polygon. This step ensured that all data were restricted to the official study area and shared identical spatial extents.

After clipping, each thematic dataset was aggregated to the census tract level using the Spatial Join tool. The join operation was set to One-to-one with the Intersect match option,

allowing point features to be summarized within their respective census tracts. For the earthquake layer, the number of earthquake events and the mean earthquake magnitude were calculated. For the school layer, the number of schools per tract was summarized. The traffic layer was processed to obtain the mean traffic volume for each tract, and the water injection layer was used to compute the mean daily injection rate. These spatial joins resulted in intermediate layers named *Tract\_EQ\_Joined*, *Tract\_School\_Joined*, and *Tract\_Traffic\_Joined*.

Finally, all layers were merged into a single integrated dataset named *OK\_Census2010\_Integrated*, which contains the summarized attributes for each census tract in Oklahoma. This layer represents the foundational dataset for subsequent analysis of earthquake risk in 2010. The final integrated map of Oklahoma census tracts is shown in *Figure 21*, which displays the complete spatial coverage of the study area and confirms that all integrated data fall within the state boundary.

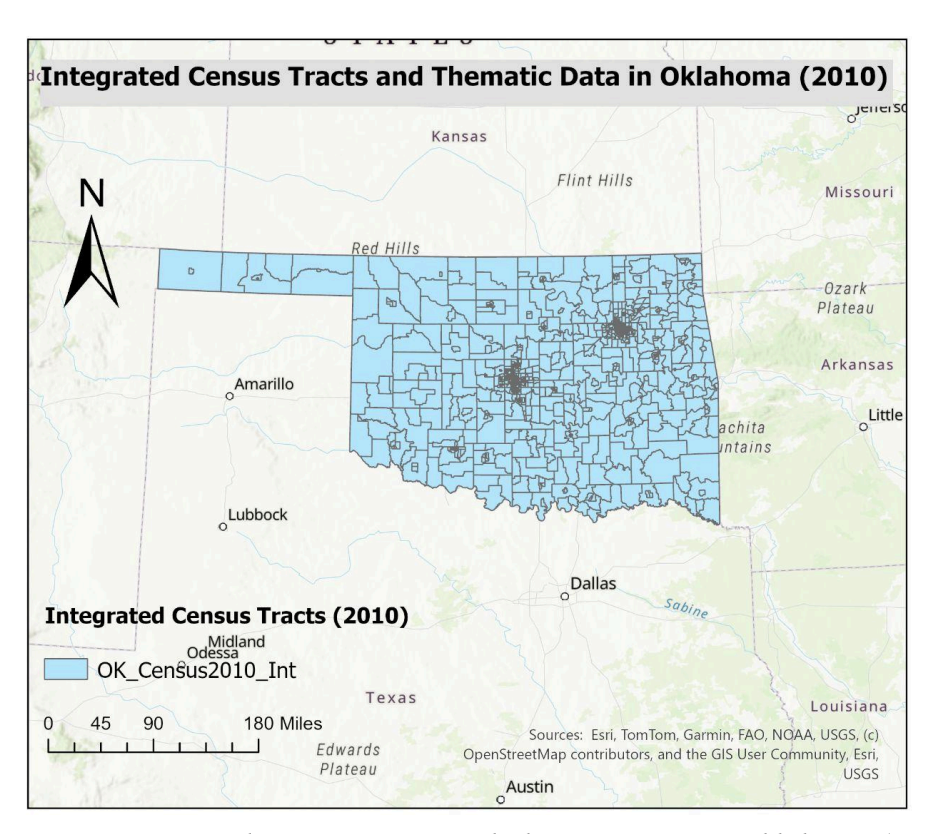


Figure 21. Integrated Census Tracts and Thematic Data in Oklahoma (2010)

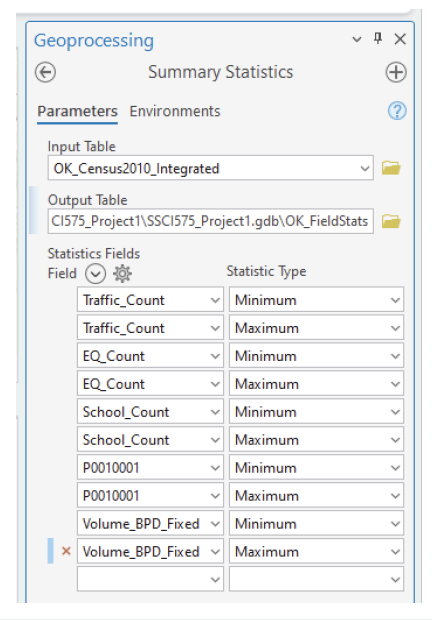
### 4 (b) Defining Scaled Indices for Each Variable

To normalize all variables and allow meaningful comparison across different magnitudes, a scaled index was defined for each dataset using the standard formula (value – minimum) divided by (maximum – minimum). The attribute table of the integrated dataset named  $OK\_Census2010\_Integrated$  was opened, and five new fields were created in sequence with the data type set to Float. These new fields were  $Pop\_Index$ ,  $Traffic\_Index$ ,  $EQ\_Index$ ,  $School\_Index$ , and  $Injection\_Index$ , representing the normalized ratios of population, traffic count, earthquake frequency, school count, and injection volume, respectively (Figure 22).

✓	Pop_Index	Pop_Index	Float
✓	Traffic_Index	Traffic_Index	Float
✓	EQ_Index	EQ_Index	Float
✓	School_Index	School_Index	Float
✓	Injection_Index	Injection_Index	Float

Figure 22. Newly added index fields in the attribute table of OK\_Census2010\_Integrated

To determine the value ranges required for standardization, the Summary Statistics tool was applied to the integrated table with five selected variables: P0010001, Traffic\_Count, EQ\_Count, School\_Count, and Volume\_BPD\_Fixed. Both minimum and maximum statistics were calculated for each variable, and the resulting output table, named OK\_FieldStats, summarized the minimum and maximum values used in the subsequent normalization process. The results indicated that the minimum and maximum of P0010001 were 31 and 12083, the minimum and maximum of Traffic\_Count were 0 and 78658, the minimum and maximum of EQ\_Count were 0 and 133, the minimum and maximum of School\_Count were 0 and 8, and the minimum and maximum of Volume\_BPD\_Fixed were 0 and 12000 (Figure 23, Table 1).



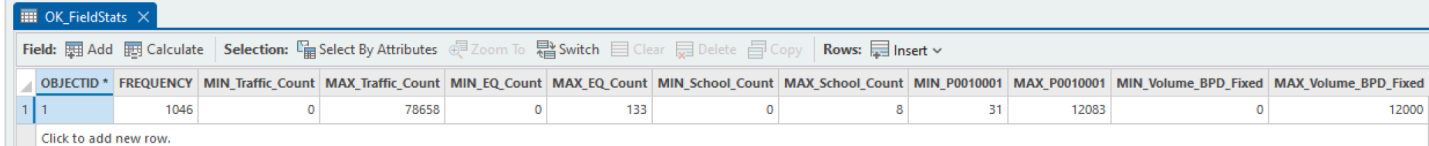


Figure 23. Summary Statistics tool interface showing selected fields and output table OK FieldStats.

Using these reference values, each of the five new index fields was calculated with the Field Calculator tool by entering the appropriate Python expressions. For the population, the expression was written as "(!P0010001! - 31.0) / (12083.0 - 31.0)" to scale the population variable between 0 and 1. Similarly, traffic count was calculated as " $(!Traffic\_Count! - 0.0) / (78658.0 - 0.0)$ ", earthquake frequency was calculated as " $(!EQ\_Count! - 0.0) / (133.0 - 0.0)$ ", and school count was calculated as " $(!School\_Count! - 0.0) / (8.0 - 0.0)$ ". The injection volume required special handling due to the presence of Null values in the original data. To avoid calculation errors, a Python function was written within the Field Calculator using a code block that first checked whether the input value was None. If it was not None, the formula "(value - 0.0) / (12000.0 - 0.0)" was applied to calculate the  $Injection\_Index$ ; otherwise, the field was set to Null.

After applying all expressions, the resulting index values were examined and confirmed to fall within the range of 0 to 1, representing the relative proportion of each variable within the study area. Records with missing injection data were automatically assigned Null values, which did not affect subsequent analyses. This process successfully produced five standardized indices that provide a consistent basis for the construction of the composite index in the following step (Figure 24).

Pop_Index	Traffic_Index	EQ_Index	School_Index	Injection_Index
0.372884	0	0.18797	0.625	<null></null>
0.179887	0	0.142857	0	<null></null>
0.384252	0.367884	0.330827	0.625	0
0.60156	0.024918	0.135338	0	0
0.692665	0.021053	0.150376	0	0
0.357368	0.207086	0.18797	0.25	0
0.636658	0.060019	0.255639	0.125	0.01475

Figure 24. Resulting standardized index values for population, traffic, earthquake, school, and injection variables.

### 4 (c) Define the final risk index by adding all the indexes computed in the previous step.

The final risk index was designed to represent the overall exposure level of each census tract by integrating five standardized indicators derived in the previous step: population density (Pop\_Index), traffic volume (Traffic\_Index), earthquake frequency (EQ\_Index), school density (School\_Index), and water injection volume (Injection\_Index). A new floating-point field named Final\_Risk\_Index was added to the attribute table of OK\_Census2010\_Integrated, with six decimal places to ensure sufficient precision. The calculation was performed using the Field Calculator in Python mode, applying a custom function that summed all available indices while automatically excluding any null values.

The Python expression used was calc\_final(!Pop\_Index!, !Traffic\_Index!, !EQ\_Index!, !School Index!, !Injection Index!).

The corresponding code block was defined as follows:

```
def calc_final(p, t, e, s, i):
    vals = [v for v in [p, t, e, s, i] if v is not None]
    if len(vals) == 0:
        return None
    else:
        return sum(vals) / len(vals)
```

This function ensured that missing data did not cause computational errors and that the resulting risk index remained scaled between 0 and 1. After running the calculation, the resulting Final\_Risk\_Index values ranged approximately from 0.02 to 0.52. Higher index values represent census tracts that experience greater combined exposure to human activity and potential environmental stressors.

Figure 25 illustrates the spatial distribution of the final risk index across Oklahoma. The map employs a graduated color ramp ranging from light yellow (lowest risk) to dark red (highest risk). The results show that areas located in northern and central Oklahoma tend to have relatively higher risk values, while peripheral regions exhibit lower overall exposure. This composite risk visualization provides a comprehensive overview of spatial vulnerability patterns across the state, integrating demographic, infrastructural, and environmental factors.

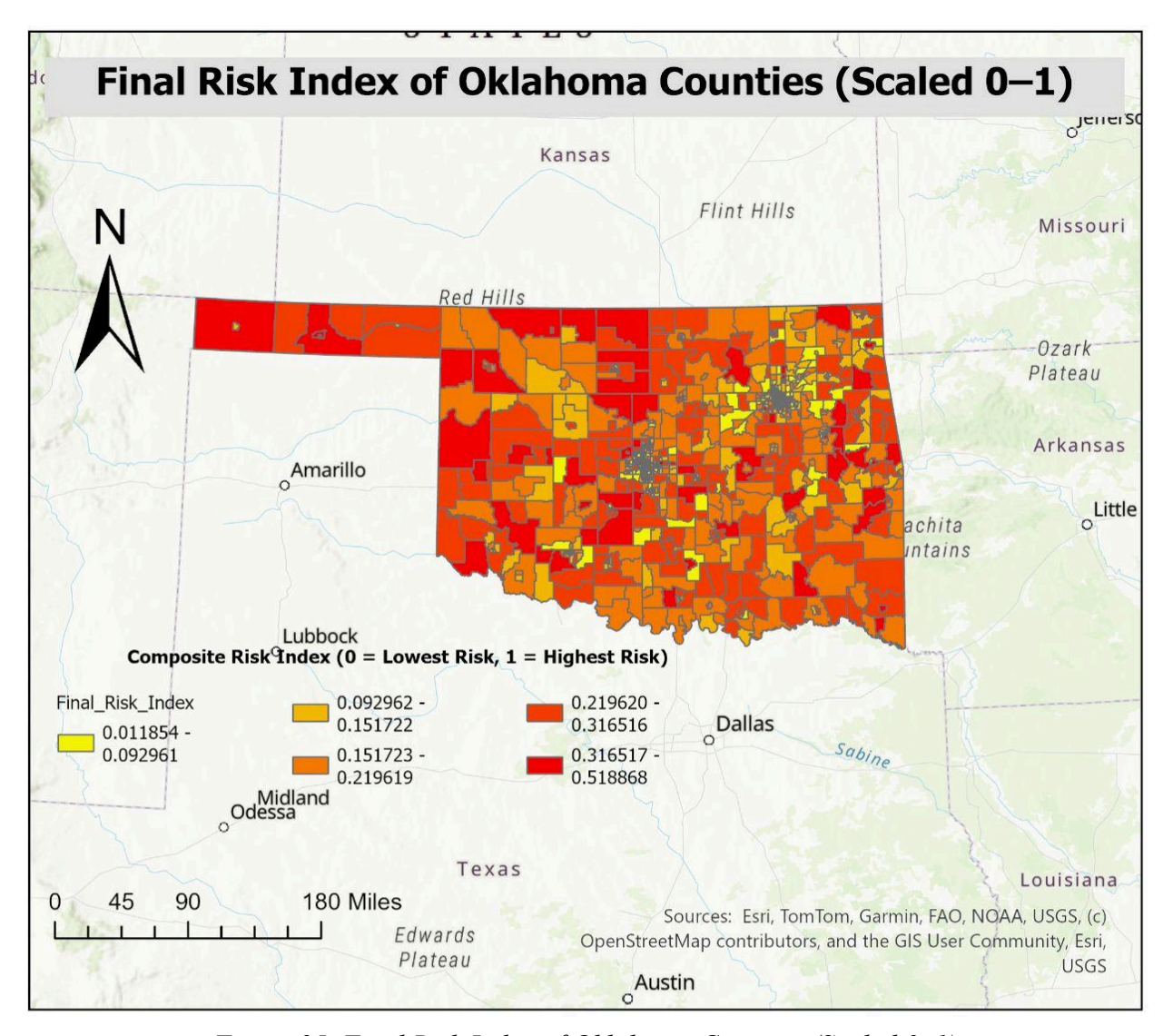


Figure 25. Final Risk Index of Oklahoma Counties (Scaled 0–1)

#### References

Fountain, H. (2015, July 3). Huge study linking wastewater injection wells to earthquakes.

Science. Retrieved October 7, 2025, from

https://www.science.org/content/article/huge-study-links-wastewater-injection-wells-eart hquakes

U.S. Geological Survey. (n.d.). Earthquake catalog data (ComCat). U.S. Department of the Interior. Retrieved October 7, 2025, from <a href="https://earthquake.usgs.gov/data/comcat/data-eventterms.php">https://earthquake.usgs.gov/data/comcat/data-eventterms.php</a>

Oklahoma Corporation Commission. (n.d.). Oklahoma underground injection well data.

Retrieved October 7, 2025, from

https://oklahoma.gov/occ/divisions/oil-gas/oil-gas-data.html